

Validity of the fluid description of critical β and Alfvén time scale of ballooning instability onset in the near-Earth collisionless high- β plasma

Akira Miura

Department of Earth and Planetary Science, University of Tokyo, Tokyo, Japan

Received 6 March 2003; revised 22 October 2003; accepted 17 November 2003; published 24 February 2004.

[1] For a realistic, highly stretched, two-dimensional tail configuration, in which the pressure gradient force is balanced with the curved field line tension force at the equator, the growth rates and the real frequencies of the ideal magnetohydrodynamic (MHD) and two component fluid (nonideal MHD) ballooning modes, in which the phrase “two component fluid” means that the Hall and the electron pressure gradient terms are included in the generalized Ohm’s law, the ion bounce frequency ω_{bi} , the ion magnetic drift frequency ω_{di} , the ion diamagnetic drift frequency ω_{*i} , and the ion cyclotron frequency ω_{ci} are calculated numerically at the equator as a function of X from the near-Earth tail ($X = -15 R_E$) to the midtail ($X = -30 R_E$). Contrary to the well-known dipole field case, in which the bounce frequency decreases with increasing $|X|$, the ion bounce frequency increases with $|X|$ for the tail configuration. The ion magnetic drift frequency dominated by the curvature drift frequency also increases with increasing $|X|$. The exact growth rates of the ideal and nonideal ballooning modes, γ_e and γ_{ne} , which are nearly equal, are given by $1.22 V_A/R_c$, where V_A is the Alfvén velocity and R_c is the field line curvature radius at the equator, and satisfy $\omega_{bi}, \omega_{di}, \omega_{*i} < \gamma_e < \omega_{ci}$ on average in the near-Earth tail at $X \sim -15 R_E$. Also, the ion motion remains adiabatic in the near-Earth tail at $X \sim -15 R_E$. Therefore it is a posteriori verified that the fluid or MHD description of the linear stability of the ballooning instability is valid, and the critical β and the Alfvén time scale $\tau_A \sim R_c/V_A$ of the ballooning instability onset obtained by the fluid theory are validated in the near-Earth tail as close as $15 R_E$ from the Earth. Despite the plasma being collisionless and high- β in the near-Earth tail, the subtle collisionless kinetic effects due to the field line curvature in high- β collisionless plasma are not significant enough to invalidate the fluid description in the near-Earth tail. The Alfvén time scale of an e-folding growth of the Alfvén wave trapped within R_c in the equatorial region is of the order of a few tens of seconds or less in the near-Earth tail. It is faster than the bounce time of the bulk of ions and can explain the observed rapid time scale of a substorm onset. There is excellent agreement between the critical β and the Alfvén time scale obtained analytically for the two component fluid plasma and those obtained by a three-dimensional particle simulation. **INDEX TERMS:** 2752 Magnetospheric Physics: MHD waves and instabilities; 7827 Space Plasma Physics: Kinetic and MHD theory; 2740 Magnetospheric Physics: Magnetospheric configuration and dynamics; 2744 Magnetospheric Physics: Magnetotail; 2788 Magnetospheric Physics: Storms and substorms; **KEYWORDS:** ballooning instability, MHD description, collisionless high-beta plasma, Alfvén time scale, near-Earth tail, substorm onset

Citation: Miura, A. (2004), Validity of the fluid description of critical β and Alfvén time scale of ballooning instability onset in the near-Earth collisionless high- β plasma, *J. Geophys. Res.*, 109, A02211, doi:10.1029/2003JA009924.

1. Introduction

[2] The rapid onset of a magnetospheric substorm characterized by a sudden increase in the brightness of auroral arcs in the premidnight region has been an enigma in space plasma physics since the early era of space exploration. At

the onset the local auroral luminosity doubles within several tens of seconds, and therefore the onset time scale (onset time constant), defined as an e-folding time scale of the rapid increase in the brightness, is of the order of several tens of seconds (see section 8.3). Although there still remains some uncertainty owing to the field line mapping problem, the onset of a substorm has been found, by extensive observations, to take place within $10 R_E$ from the Earth [e.g., Lopez *et al.*, 1990; Samson *et al.*, 1992;

Jacquay et al., 1991; *Erickson et al.*, 2000; *Frank and Sigwarth*, 2000; *Liou et al.*, 2002; *Dubyagin et al.*, 2003]. Such a region so close to the Earth is unlikely to be subject to reconnection, and therefore what physical mechanism causes a rapid onset and under what physical conditions and what parameters of the near-Earth plasma sheet determine the rapid onset time scale have been critical issues of the substorm onset problem.

[3] Ballooning instability, which is a pressure-driven instability growing in a fast magnetohydrodynamic (MHD) time scale, was originally found in fusion plasmas (see *Coppi* [1977] and references therein). It is quite likely that the near-Earth plasma sheet, where the plasma β (ratio of plasma to magnetic pressure) is high and there is an earthward pressure gradient with an unfavorable field line curvature, is subject to ballooning instability. Although solution of the ballooning equation is quite difficult analytically because of its awkward dependence on the explicit form of the equilibrium, a realistic near-Earth tail has been shown to be ballooning unstable by a numerical eigenmode analysis [*Miura et al.*, 1989] and also a numerically created outer edge of the ring current has been shown to be subject to a pressure driven instability [*Ohtani et al.*, 1989]. *Wu et al.* [1998] showed by a three-dimensional (3-D) linear MHD stability analysis of the 2-D static equilibrium in the plasma sheet that the equilibrium configuration is subject to a pressure driven instability. *Lee* [1998] also showed that an analytic model equilibrium or the 2-D plasma sheet that includes the Earth's 2-D dipole field is subject to ballooning instability. Although an exact MHD equilibrium was not used, *Bhattacharjee et al.* [1998] showed by an eigenmode analysis that a 2-D magnetotail is subject to ballooning instability. A full particle simulation of *Pritchett and Coroniti* [1999] clearly demonstrated growth of ballooning instability in the near-Earth plasma sheet.

[4] In a highly stretched tail configuration in the near-Earth plasma sheet appearing prior to a substorm onset, the growth time (the e-folding time) of ballooning instability can be as short as the field line curvature radius at the equator (R_c) divided by the Alfvén velocity at the equator (V_A), which is the Alfvén time scale ($\tau_A \sim R_c/V_A$) of a strongly localized Alfvén wave trapped in the equatorial region within a curvature radius of the field line at the equator [*Miura*, 2000]. For typical parameters prior to the onset such as $R_c \sim 10,000$ km and $V_A \sim 1000$ km/s, the growth time or τ_A becomes a few tens of seconds. Therefore if the magnetotail could somehow put itself in a highly stressed state passing through the marginal state rapidly, this rapid linear growth of ballooning instability would explain the rapid onset of a substorm. However, in a curved field line geometry in high- β plasma, such as magnetic confinement devices in fusion plasmas and the magnetotail, subtle collisionless effects exist and the application of fluid treatment based on the localization of wave-plasma interaction, cannot be guaranteed unless $\omega_b, \omega_d, \omega_* < |\omega|$ is satisfied on average, where ω is the frequency of the ballooning disturbance, ω_b and ω_d are the bounce and the magnetic gradient-curvature drift frequencies of particles, respectively, and ω_* is the diamagnetic drift frequency [*Hurricane et al.*, 1994; *Horton et al.*, 2001; *Le Contel et al.*, 2001].

[5] When the above condition is not satisfied, the particles cannot be treated as a fluid and a kinetic approach

such as μ -conserving gyrokinetics [*Tang and Catto*, 1981; *Chen and Hasegawa*, 1991] is necessary. This is because if $\omega_b < |\omega|$ is not satisfied, the particles bounce back and forth many times during the wave growth and the electric field which particles feel is the bounce-averaged one (nonlocal response), which differs greatly from the local one used in the fluid description. Although the early numerical eigenmode analysis of ballooning instability has shown that the growth time indeed becomes of the order of 10 s for a realistic near-Earth tail model [*Miura et al.*, 1989], the above condition for the validity of fluid treatment has not been tested.

[6] The purpose of this paper is to calculate ω_b, ω_d , and ω_* for ions in the same near-Earth tail model as used by *Miura et al.* [1989] and to show a posteriori that $|\omega| > \omega_b, \omega_d, \omega_*$ is indeed satisfied on average and thus ion dynamics which are essential for excitation of ballooning instability can indeed be described by fluid equations as described by *Miura et al.* [1989]. The condition $|\omega| < \omega_{ci}$, which may guarantee the quasi-neutrality assumption in the MHD, where ω_{ci} is the ion gyrofrequency, is also verified. The critical plasma β (β_{cr}) and the plasma β for the same tail model are also calculated at the equator to show that $\beta > \beta_{cr}$. Therefore the necessary condition for the instability is indeed satisfied for a stretched tail configuration in the near-Earth tail. Here, in calculation of $|\omega|$ and β_{cr} we assume the incompressibility of the plasma, which replaces the equation of state. The present fluid approach is not a kinetic approach valid for collisionless plasmas such as has been pursued for a self-consistent field and plasma model including the dipole field component [*Horton et al.*, 2001]. However, subtle collisionless features described above are shown not to be important for ions near at least $X \sim -15 R_E$, although it becomes important with increasing $|X|$, where GSM coordinates are used and X is pointing sunward. Since the present tail model does not include the dipole field in the near-Earth region, the present calculation cannot be extended to the near-Earth in $|X| < 15 R_E$. Although the above condition is not satisfied for electrons, we use a generalized Ohm's law to describe the electron dynamics. For such a low-frequency ion-driven mode, the ion dynamics practically govern the instability growth, although electron kinetics such as the electron trapping effect [*Cheng and Lui*, 1998] may be important.

[7] There are suggestions of ballooning instability as a mechanism causing Earth's substorms [e.g., *Roux et al.*, 1991; *Erickson et al.*, 2000]. The ballooning instability is in principle viable in any high- β planetary magnetosphere with inward directed ∇p and an unfavorable curvature of the field line, and it has indeed been studied in the Jovian magnetosphere, which is rapidly rotating [*McNutt et al.*, 1987].

[8] In the following, the validity of the incompressible assumption for ballooning instability in high- β ($\beta \gg 1$) plasma is revisited in section 2. The growth rates and frequencies of ballooning modes are obtained for the ideal MHD and two component fluid plasma in section 3. A realistic tail model used in the present calculation is explained in section 4. The formulae of the bounce frequency and the magnetic gradient-curvature drift frequency are given in section 5. Numerical results are presented in section 6. The validity of the fluid description of ballooning

instability onset is discussed in section 7. A discussion is presented in section 8. A summary and a conclusion are given in section 9.

2. Validity of the Incompressible Assumption for Ballooning Instability in the High β ($\beta \gg 1$) Near-Earth Tail Revisited

[9] In the eigenmode analysis of ballooning instability in the near-Earth plasma sheet [Miura *et al.*, 1989] the incompressible assumption was introduced without proving its validity. Subsequently, for an ideal MHD plasma, Miura [2000] has shown by calculation of an energy functional for an exponential trial function that a ballooning mode which is strongly confined in high- β ($\gg 1$) plasma near the equator is incompressible. When the field line curvature radius R_c becomes comparable to the ion Larmor radius near the equator, the ion motion becomes stochastic and μ conservation is violated [Büchner and Zelenyi, 1989; Chen, 1992], and so the adiabatic equation of state is not valid [Hurricane *et al.*, 1995]. However, for stochastic plasma, Miura [2000] has also shown by using the MHD-like formulation of Hurricane *et al.* [1995] that a ballooning mode strongly localized near the equator is essentially incompressible irrespective of the β value, that is, the equation of state for stochastic plasma can be replaced by a robust mechanical equation $\nabla \cdot \delta \mathbf{u} = 0$. In this section the validity of the incompressible assumption for a low-frequency perturbation ($|\omega| \sim |k_{\parallel} V_A|$), where k_{\parallel} and V_A are the parallel wave number and the Alfvén velocity at the equator, respectively, and for high- β ($\beta \gg 1$) plasma near the equator, which necessarily means a highly stretched tail configuration, is proved in a somewhat different manner from the equation of motion.

[10] In the 2-D equilibrium we obtain [Freidberg and Marder, 1973; Horton *et al.*, 1999; Miura, 2000]

$$\omega^2 \rho_0 \delta u_{\parallel} = -\Gamma p_0 (\mathbf{e} \cdot \nabla) (\nabla \cdot \delta \mathbf{u}), \quad (1)$$

where δu_{\parallel} is the parallel velocity perturbation, \mathbf{e} is the unit vector parallel to the unperturbed magnetic field, Γ is the ratio of specific heat, and ρ_0 and p_0 are unperturbed plasma density and pressure, respectively. Equation (1) can be rewritten as

$$\omega^2 \rho_0 \delta u_{\parallel} = -\Gamma p_0 (\mathbf{e} \cdot \nabla) [\nabla \cdot \delta \mathbf{u}_{\perp} + B_0 \mathbf{e} \cdot \nabla (\delta u_{\parallel} / B_0)]. \quad (2)$$

[11] Let us consider a strongly localized ballooning mode with a nonzero k_{\parallel} . Then, if

$$|\omega^2 \rho_0 \delta u_{\parallel}| \ll |\Gamma p_0 k_{\parallel}^2 \delta u_{\parallel}|, \quad (3)$$

that is, if

$$\omega^2 \ll C_s^2 k_{\parallel}^2, \quad (4)$$

where C_s is the sound speed, the second term in the right-hand side of equation (2) is much larger than the left-hand side. If we assume that the ballooning mode is essentially in the Alfvén branch, the substitution of $|\omega^2| \sim |k_{\parallel}^2 V_A^2|$, the validity of which should be justified a posteriori after we obtain the growth rate, into equation (4) yields $\beta \gg 1$.

Therefore for $\beta \gg 1$ the left-hand side of equation (2) is much smaller than the second term in the right-hand side of equation (2). Since the second term of the right-hand side of equation (2) is equal to $\nabla \cdot (\delta u_{\parallel} \mathbf{e})$, this means that for $\beta \gg 1$,

$$|\nabla \cdot \delta \mathbf{u}| \ll |\nabla \cdot (\delta u_{\parallel} \mathbf{e})|. \quad (5)$$

This means that $|\nabla \cdot \delta \mathbf{u}|$ is much smaller than one of its constituent term. This condition is possible only when $\nabla \cdot \delta \mathbf{u} \sim 0$. Therefore when $\beta \gg 1$, the incompressible assumption $\nabla \cdot \delta \mathbf{u} \sim 0$ is valid for a low-frequency ballooning perturbation $|\omega| \sim |k_{\parallel} V_A|$. This provides further proof of the validity of the incompressible assumption ($\nabla \cdot \delta \mathbf{u} = 0$) for ballooning instability in $\beta \gg 1$ plasma.

[12] For the ideal MHD plasma the above result is consistent with the minimizing condition of the potential energy in the MHD energy principle [Bernstein *et al.*, 1958; Freidberg, 1987], which says that the most unstable mode satisfies

$$\mathbf{e} \cdot \nabla (\nabla \cdot \delta \mathbf{u}) = 0. \quad (6)$$

The validity of the incompressible assumption may also be justified empirically by the condition that $V_{*i} \ll V_A$, C_s , where V_{*i} is a macroscopic velocity, i.e., the ion diamagnetic drift velocity, which is calculated in the next section. We will find in Figure 3 that $V_{*i} \sim 65$ km/s $\ll V_A$ is valid at $|X| < 24 R_E$ and also V_{*i} is much smaller than $C_s = 1230$ km/s for $kT_i = kT_e = 4.71$ keV used in the present calculation (see section 4).

[13] In short, high- β ($\beta \gg 1$) plasma can be perturbed so as not to compress the plasma for a low frequency ballooning perturbation $|\omega| \sim |k_{\parallel} V_A|$. This means that although the compressibility is an important stabilizing factor for an interchange mode [Gold, 1959], which has $k_{\parallel} \sim 0$, the compressible stabilization is not important for ballooning instability in high- β ($\gg 1$) plasma [Miura, 2000, 2001] (notice that the above mathematical discussion is not valid for an interchange mode with $\mathbf{e} \cdot \nabla \sim ik_{\parallel} \sim 0$). It is important to notice here that for the study of ballooning instability in the Jovian magnetosphere [McNutt *et al.*, 1987], the condition of incompressibility has also been introduced to simplify the analysis and to replace the equation of state.

3. Ideal MHD and Two Component Fluid Ballooning Modes

[14] Since it has been observed [Lui *et al.*, 1992] that $p_{\perp} \sim p_{\parallel}$ immediately prior to a substorm onset, the isotropic pressure is assumed. According to the discussion in the previous section, ballooning modes in the ideal MHD and stochastic plasmas in a high- β tail can be described by the incompressible MHD ballooning mode equation [Miura *et al.*, 1989; Miura, 2000]

$$B_0 V_A^2 (\mathbf{e} \cdot \nabla) [B_0^{-1} (\mathbf{e} \cdot \nabla) \delta \Phi] + (\omega^2 + \gamma_{MHD}^2) \delta \Phi = 0, \quad (7)$$

where

$$\gamma_{MHD}^2 = \frac{2|\nabla p_0|}{\rho_0 R_c} \quad (8)$$

and $\delta\Phi$ is the potential perturbation, which is a function of s , the distance from the equator ($s = 0$) along the field line.

[15] The unperturbed form of a generalized Ohm's law taking into account the Hall effect and the electron pressure gradient can be written as

$$-n_0 e(\mathbf{E}_0 + \mathbf{v}_0 \times \mathbf{B}_0) + \mathbf{j}_0 \times \mathbf{B}_0 - \nabla p_{e0} = 0, \quad (9)$$

where the subscript 0 denotes the unperturbed state and p_{e0} is the unperturbed electron pressure and n_0 is the unperturbed plasma density. The unperturbed form of the equation of motion can be written as

$$\rho_0(\mathbf{v}_0 \cdot \nabla)\mathbf{v}_0 = \mathbf{j}_0 \times \mathbf{B}_0 - \nabla p_0. \quad (10)$$

Since \mathbf{v}_0 is in the east-west direction when \mathbf{E}_0 and ∇p_{e0} are in the X direction and we assume that the unperturbed state is uniform in the east-west direction, the left hand side of equation (10) vanishes. Thus one obtains from equations (9) and (10)

$$\mathbf{v}_{0\perp} = \frac{\mathbf{E}_0 \times \mathbf{B}_0}{B_0^2} + \frac{1}{n_0 e B_0} \mathbf{B}_0 \times \nabla p_{i0}. \quad (11)$$

Notice that for the ideal MHD, the second term should be nonexistent. Since we assume $\mathbf{E}_0 = 0$ in the present analysis, we obtain

$$\mathbf{v}_{0\perp} = \frac{1}{n_0 e B_0} \mathbf{e} \times \nabla p_{i0} \quad (12)$$

for the two component fluid case, which is a nonideal MHD case. This is the ion diamagnetic drift velocity (\mathbf{V}_{*i} ($= \mathbf{v}_{0\perp}$)) and is expressed by using the ion magnetization vector $\mathbf{M}_i = -e p_{i0}/B_0$ as follows:

$$en_0 \mathbf{V}_{*i} = en_0 \mathbf{V}_{gci} + \nabla \times \mathbf{M}_i, \quad (13)$$

where

$$n_0 \mathbf{V}_{gci} \equiv \int d^3 v f_i \mathbf{v}_{gci} \quad (14)$$

is the flow corresponding to guiding-center motion and \mathbf{v}_{gci} is the sum of the gradient- B and curvature drifts of an ion [e.g., *Hazeltine and Waelbroeck*, 1998]. Therefore in the two component fluid description, ω^2 in equation (7) must be replaced by $\omega(\omega - \omega_{*i})$, where

$$\omega_{*i} = \mathbf{k}_\perp \cdot \mathbf{v}_{0\perp} = \frac{1}{n_0 e B_0} \mathbf{k}_\perp \cdot (\mathbf{e} \times \nabla p_{i0}) \quad (15)$$

and $\mathbf{k}_\perp = k_y \hat{\mathbf{y}}$ is the wave number vector in the east-west direction, $\hat{\mathbf{y}}$ being the unit vector in the Y direction pointing toward the dusk. Whereas ω is a pure imaginary in the ideal MHD case, ω has a real part owing to this prescription in the two component fluid description. The ion diamagnetic drift frequency ω_{*i} is the same as $\omega_{\perp i}$ used in *Miura et al.* [1989]. This prescription of replacing ω^2 with $\omega(\omega - \omega_{*i})$ to replace the inertia term means that only the electric field perturbation arising from the frozen-in part of the generalized Ohm's law is retained, which is a good approximation

as far as the perpendicular electric field component is concerned. If the parallel component of the electric field is also taken into account, the full two component fluid ballooning mode equation taking into account the ion diamagnetic drift and the parallel electric field perturbation becomes

$$B_0 V_A^2 (\mathbf{e} \cdot \nabla) [B_0^{-1} (\mathbf{e} \cdot \nabla) \delta\Phi] + \left[\omega (\omega - \omega_{*i}) + \gamma_{MHD}^2 \right] \delta\Phi = -B_0 V_A^2 (\mathbf{e} \cdot \nabla) (B_0^{-1} \delta E_{\parallel}) \quad (16)$$

where

$$\delta E_{\parallel} = -\frac{1}{en_0} (\mathbf{e} \cdot \nabla) \delta p_e + \frac{\omega_{*e}}{k_y} \delta B_n \quad (17)$$

and

$$\omega_{*e} = -\frac{1}{n_0 e B_0} \mathbf{k}_\perp \cdot (\mathbf{e} \times \nabla p_{e0}). \quad (18)$$

Here, $\mathbf{n} = \hat{\mathbf{y}} \times \mathbf{e}$. Notice that the right-hand side of equation (16) appears owing to the parallel electric field in the generalized Ohm's law arising from ∇p_e , which is given by equation (17). Substitution of $\delta B_n = ik_y \delta A_{\parallel} = (k_y/\omega)[(\mathbf{e} \cdot \nabla) \delta\Phi + \delta E_{\parallel}]$ into equation (17) yields $\delta E_{\parallel} \sim -(\mathbf{e} \cdot \nabla) \delta p_e / (n_0 e)$ when $|\omega| \gg |\omega_{*e}|$, which is satisfied in the present calculation (see Figure 9). Then, if we assume that the right-hand side of equation (16) is small compared with the left-hand side of equation (16), we obtain a two component fluid ballooning mode equation

$$B_0 V_A^2 (\mathbf{e} \cdot \nabla) [B_0^{-1} (\mathbf{e} \cdot \nabla) \delta\Phi] + \left[\omega (\omega - \omega_{*i}) + \gamma_{MHD}^2 \right] \delta\Phi = 0. \quad (19)$$

The above procedure means that although δE_{\parallel} given by equation (17) is important for particle acceleration (auroral electron acceleration), its effect is assumed unimportant for $|\omega| \gg |\omega_{*e}|$ in equation (16), which is originally derived from $\nabla \cdot \delta \mathbf{j} = 0$ [*Miura et al.*, 1989].

[16] Since the scale length L_B over which B_0 changes appreciably at $s = 0$ is infinite ($L_B^{-1} = B_0^{-1} dB_0/ds = 0$ at $s = 0$), we can assume $\mathbf{e} \cdot \nabla = ik_{\parallel}$ ($k_{\parallel} L_B \gg 1$) at $s = 0$ and the dispersion equation of equation (19) becomes approximately

$$\omega^2 - \omega_{*i} \omega + \gamma_{MHD}^2 - k_{\parallel}^2 V_A^2 = 0. \quad (20)$$

Since L_B varies extremely rapidly across $s = 0$, the above eikonal approximation is not well justified at the midplane of a realistic magnetotail and a more exact analysis will be required in the future. The frequency obtained from equation (20) is given by

$$\omega = \frac{\omega_{*i} \pm \sqrt{\omega_{*i}^2 - 4(\gamma_{MHD}^2 - k_{\parallel}^2 V_A^2)}}{2}. \quad (21)$$

The ballooning instability occurs when

$$\gamma_{MHD}^2 > k_{\parallel}^2 V_A^2 + \frac{\omega_{*i}^2}{4}. \quad (22)$$

Notice that the second term in the right-hand side of equation (22) is a correction term due to the ion diamagnetic drift in the two component fluid description.

[17] For the ideal MHD case, equation (21) gives

$$\gamma^2 = \gamma_{MHD}^2 - k_{\parallel}^2 V_A^2, \quad (23)$$

where $\omega = \omega_r + i\gamma$ and $\omega_r = 0$. The low frequency assumption $|\omega| \sim |k_{\parallel} V_A|$, the validity of which should be justified a posteriori after the growth rate is obtained, yields

$$\gamma^2 \sim k_{\parallel}^2 V_A^2 \sim \frac{1}{2} \gamma_{MHD}^2. \quad (24)$$

Therefore we obtain

$$\gamma \sim \frac{1}{\sqrt{2}} \gamma_{MHD}. \quad (25)$$

[18] The force balance of the static tail configuration gives

$$\nabla_{\perp} p_0 = \mu_0^{-1} B_0^2 (\kappa_c - \kappa_b), \quad (26)$$

where $\kappa_c = (\mathbf{e} \cdot \nabla) \mathbf{e}$ and $\kappa_b = \nabla_{\perp} \ln B_0$. For a highly stretched tail configuration used in the present study, $|\kappa_c| \gg |\kappa_b|$ is valid near $s = 0$. Therefore near the equatorial plane, equation (26) becomes approximately

$$\nabla_{\perp} p_0 \sim \mu_0^{-1} B_0^2 \kappa_c. \quad (27)$$

Substitution of equation (27) into equation (8) and using equation (25) yields the growth rate of the ballooning mode, which is strongly localized near the equator

$$\gamma \sim \frac{1}{\sqrt{2}} \gamma_{MHD} \sim \frac{V_A}{R_c}, \quad (28)$$

where V_A and R_c are the Alfvén speed and field line curvature radius at the equator, respectively. Since the low-frequency assumption $|\omega| \sim |k_{\parallel} V_A|$ has been adopted, the comparison of equation (28) and $|\gamma| \sim |k_{\parallel} V_A|$ shows that the low-frequency assumption is justified a posteriori if the local parallel wave number at the equator $k_{\parallel} = 1/R_c$.

[19] Therefore from equations (8) and (22), the ballooning mode occurs in the ideal MHD, when

$$\beta > \beta_{cr} = k_{\parallel}^2 L_p R_c = \frac{L_p}{R_c}, \quad (29)$$

where β is defined at the equator and equal to $2\mu_0 p_0 / B_0^2$, β_{cr} is the critical β for the ideal MHD ballooning mode, and $L_p^{-1} = |\nabla p_0| / p_0$ at the equator.

[20] For the two-component fluid case (nonideal MHD case), substitution of equations (8) and (15) and $k_{\parallel} = 1/R_c$ into equation (21) yields an unstable mode with

$$\omega_m = \frac{1}{2} \omega_{*i} = \frac{k_y |\nabla p_{i0}|}{2n_0 e B_0} \quad (30)$$

$$\gamma_n = \left[\frac{2|\nabla p_0|}{\rho_0 R_c} - \frac{V_A^2}{R_c^2} - \frac{1}{4} \left(\frac{k_y |\nabla p_{i0}|}{n_0 e B_0} \right)^2 \right]^{1/2}, \quad (31)$$

where the subscript n means the nonideal MHD. In this case the unstable mode occurs when

$$\beta > \beta_{crn} = \beta_{cr} + \frac{\omega_{*i}^2 R_c L_p}{4V_A^2} = \beta_{cr} \left(1 + \frac{\omega_{*i}^2 R_c^2}{4V_A^2} \right), \quad (32)$$

where β_{crn} is the critical β for the two component fluid (nonideal MHD) ballooning instability.

4. A Model of the Near-Earth to Mid Tail

[21] Figure 1 shows magnetic field lines in the tail model used by *Miura et al.* [1989], which was originally used by *Kan* [1973] to study the tail structure. Since it does not include the dipole field in the near-Earth region, we use this model (a solution of the Vlasov-Maxwell equations) to describe the magnetic field and plasma in the near-Earth to mid tail from $X = -15 R_E$ to $X = -30 R_E$. Here, Z is directed to the north and $Z = 0$ is the equatorial plane. Except for the region close to the Earth at $|X| < 15 R_E$ this stretched tail configuration may represent the near-Earth to mid tail in the late growth phase prior to a substorm onset, when the field lines in the tail are highly stretched tailward. In order to make this tail model realistic, we chose a reference point at $X = -20 R_E$ and $Z = 0$, where the Z component of the unperturbed magnetic field B_{0Z} is set nearly equal to an observed value $B_{0Z} = 1.37$ nT [Fairfield, 1987]. In the real magnetotail, T_i is much larger than T_e . However, we assumed uniform and equal ion and electron temperatures as in Kan's original tail model and assumed specifically $kT_i = kT_e = 4.71$ keV. Then, in order to have a pressure comparable to observations at $X = -20 R_E$ we assume $n_0 = 4.38 \times 10^{-2} \text{cm}^{-3}$, which is the unperturbed density at $X = -20 R_E$ and $Z = 0$. Although n_0 turned out to be much smaller than the observed value, the calculated pressure and β at $X = -20 R_E$ are comparable to those observed values near $X = -20 R_E$.

[22] Although the field model at $|X| < 15 R_E$ is not a good model, we show in Figure 1 field lines up to $|X| \sim 12 R_E$. This is because these field lines at $|X| < 15 R_E$ are necessary to calculate the bounce frequency of ions at $|X| \sim 15 R_E$. The field model shown in Figure 1 for $|X| < 15 R_E$ is not accurate but is sufficient for calculation of the bounce frequency, since the mirror points for thermal ions with $kT_i = 4.71$ keV occur close to $s \sim 0$.

5. Bounce Frequency and Magnetic Gradient-Curvature Drift Frequency

[23] Since the ballooning mode is strongly localized near the equator, the fluid description of the ion kinetics in the ballooning mode is valid when ω_{bi} , ω_{di} , $\omega_{*i} < |\omega| < \omega_{ci}$ is satisfied on average at the equator. In the following we use the ion thermal speed v_{ti} defined by $v_{ti} = (2kT_i/m_i)^{1/2}$ and the pitch angle θ_{eq} at the equator.

[24] The ion bounce time τ_{bi} of the thermal speed ion is given by

$$\tau_{bi} = \frac{4}{v_{ti}} \int_0^{s_m} \frac{ds}{[1 - B(s)/B_m]^{1/2}}, \quad (33)$$

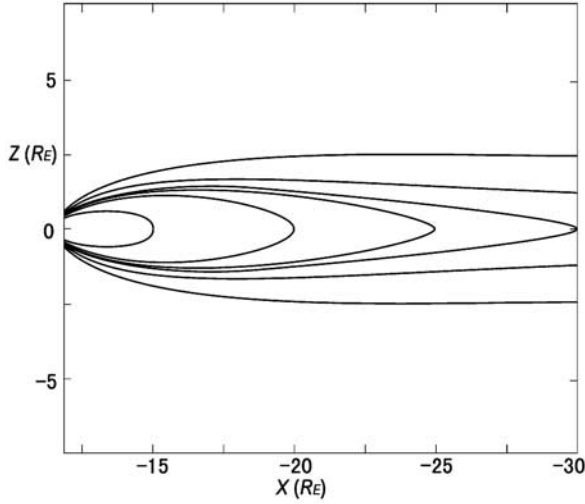


Figure 1. A model of the near-Earth to mid tail. Different field lines are plotted.

where s is the distance along the field line from the equator ($s = 0$). The magnetic field strength at the mirror point is denoted by B_m and it is a function of X , v_{ti} and θ_{eq} , and s_m is the distance from the equator to the mirror point along the field line. Notice that this formula is obtained by assuming that the first invariant $\mu = m_i v_{\perp}^2 / (2B_0)$ of an ion is conserved during the bouncing motion. The ion bounce time τ_{bi} for a particular field line is the function of X , v_{ti} and θ_{eq} . Using τ_{bi} , we obtain the ion bounce frequency

$$\omega_{bi} = \frac{2\pi}{\tau_{bi}}. \quad (34)$$

[25] The magnetic gradient-curvature drift velocity of an ion is given by

$$\mathbf{v}_{di} = \frac{\mathbf{e}}{\omega_{ci}} \times \left(v_{\parallel}^2 \boldsymbol{\kappa}_c + \frac{\mu}{m_i} \nabla B_0 \right). \quad (35)$$

Therefore the magnetic gradient-curvature drift frequency ω_{di} at the equator is defined by

$$\omega_{di} = \mathbf{k}_{\perp} \cdot \mathbf{v}_{di} = \frac{k_y}{\omega_{ci}} \left(v_{\parallel}^2 |\boldsymbol{\kappa}_c| + \frac{v_{\parallel}^2}{2} |\boldsymbol{\kappa}_b| \right). \quad (36)$$

This can be rewritten as

$$\omega_{di} = \frac{k_y}{\omega_{ci}} v_{ti}^2 \left(\frac{\cos^2 \theta_{eq}}{R_c} + \frac{\sin^2 \theta_{eq}}{2R_b} \right), \quad (37)$$

where $R_c = |\boldsymbol{\kappa}_c|^{-1}$ and $R_b = |\boldsymbol{\kappa}_b|^{-1}$ at the equator.

[26] The east-west wave number k_y in equation (37) is arbitrary in the present local treatment. However, in the actual 3-D nonlocal problem, the growth rate is expected to be maximized at some wavenumber $k_y = k_{ym}$. Since the present analysis described in section 3 assumes a local approximation in the \mathbf{n} direction, k_{ym} is not self-consistently determined. However, since the ballooning instability is

driven by the radial pressure gradient, which has a scale length L_p at the equator, we assume that $k_{ym} \sim L_p^{-1}$, i.e., the growth rate is maximized when $k_y L_p \sim 1$ is satisfied. Therefore in the next section we calculate ω_{di} and ω_{*i} by assuming $k_y = k_{ym} = L_p^{-1}$, where L_p is calculated from the unperturbed plasma configuration shown in Figure 1.

6. Numerical Results

[27] Figure 2 shows as a function of X the ion Larmor radius ρ_{Li} (dotted curve) for 90° pitch angle ions with the thermal speed v_{ti} , the field line curvature radius R_c (solid curve), the $\nabla_{\perp} B_0$ scale length R_b (dashed curve), and the pressure gradient scale length L_p (dot-dash curve) calculated at the equator ($Z = 0$). The curvature radius R_c is almost constant at $15 R_E < |X| < 17.5 R_E$ and then decreases gradually with an increase in $|X|$. All other scale lengths L_p , R_b , and ρ_{Li} lengthen with an increase in $|X|$. Whereas L_p increases very rapidly with $|X|$, R_b increases linearly with $|X|$. We find that $\rho_{Li} \sim R_c$ at $X = -15 R_E$ and $\rho_{Li} > R_c$ for $|X| > 15 R_E$. Therefore as far as this tail model is concerned, the stochastic effect in the sense of *Hurricane et al.* [1995] is important for 90° pitch angle ions at all X shown in Figure 2. However, for smaller pitch angle ions, ρ_{Li} becomes smaller. Therefore for those smaller pitch angle ions, the ion motion remains adiabatic near $X = -15 R_E$. Since $R_c \ll R_b$ or $|\boldsymbol{\kappa}_c| \gg |\boldsymbol{\kappa}_b|$ is valid at the equator for all X , the field line is stretched tailward strongly and the outward pressure gradient force is almost balanced with the inward directed tension force of the field line at the equator. This validates equation (27) at all X . For such a tail configuration, the incompressible assumption has been shown to be valid for the ideal MHD case as well as for the stochastic plasma case [Miura, 2000]. Since $\beta \gg 1$ at the equator at all X as we will find in Figure 4, the incompressible assumption for the ideal, two component fluid and stochastic plasmas is also validated from the discussion in section 2. Since $L_p \sim 7.36$

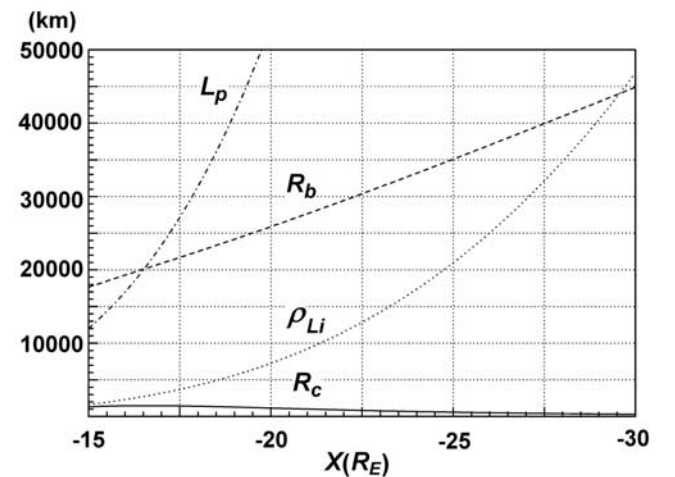


Figure 2. The ion Larmor radius ρ_{Li} (dotted curve) for 90° pitch angle ions with the thermal velocity v_{ti} , the field line curvature radius R_c (solid curve), the $\nabla_{\perp} B_0$ scale length R_b (dashed curve), and the pressure gradient scale length L_p (dot-dash curve) calculated at the equator ($Z = 0$) as a function of X .

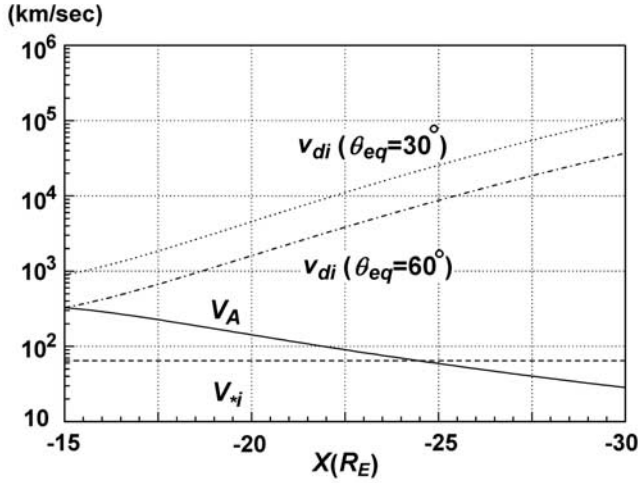


Figure 3. The ion diamagnetic drift velocity V_{*i} (dashed line), the Alfvén velocity V_A (solid line), and the magnetic gradient curvature drift velocities v_{di} for ions with the pitch angle at the equator $\theta_{eq} = 30^\circ$ (dotted line) and 60° (dot-dash line), respectively. All velocities are calculated at the equator.

ρ_{Li} at $X = -15 R_E$ from Figure 1, $k_{ym} \rho_{Li} \sim 0.136$ and this is much smaller than 1.0. Therefore the neglect of the full finite Larmor radius (FLR) effect of ions is validated.

[28] Figure 3 shows the ion diamagnetic drift velocity V_{*i} (dashed line), the Alfvén velocity V_A (solid line), and the magnetic gradient curvature drift velocities v_{di} for ions with the pitch angle at the equator $\theta_{eq} = 30^\circ$ (dotted line) and 60° (dot-dash line), respectively. All those velocities are calculated at the equator. The velocity V_{*i} is constant for all X and is nearly equal to 65 km/s. In this log-linear plot, V_A decreases linearly with $|X|$ because the normal component of the magnetic field at the equator decreases faster than the decrease of the square root of the density at the equator. The velocities v_{di} for $\theta_{eq} = 30^\circ$ and 60° increase almost linearly with $|X|$ in this log-linear plot. Since $R_c \ll R_b$ is valid at all X , the curvature drift dominates in equation (35) and therefore v_{di} is larger for $\theta_{eq} = 30^\circ$ than $\theta_{eq} = 60^\circ$.

[29] Once the unperturbed state and its scale lengths are determined, we can calculate β_{cr} and β_{crn} from equations (29) and (32), respectively. Figure 4 shows β calculated at the equator ($Z = 0$) and β_{cr} calculated by equation (29) as a function of X . This figure shows that both β (solid curve) and β_{cr} (dashed curve) increase with $|X|$. If we calculate β_{crn} by equation (32) using $k_y = k_{ym} = L_p^{-1}$, β_{crn} becomes almost equal to β_{cr} at $|X| > 15 R_E$. Therefore the curve of β_{cr} in Figure 4 also shows the curve of β_{crn} . From equations (27) and (29) we obtain for the highly stretched tail configuration

$$\beta \sim 2\beta_{cr} \quad (38)$$

at the equator. At $X = -15 R_E$, we find $\beta \sim 17$ and $\beta_{cr} \sim 9$, and so $\beta \sim 2\beta_{cr}$ is nearly satisfied.

[30] Figure 5 shows, as a function of X , γ (solid curve) calculated by equation (28), ω_{rn} (dashed curve) calculated by equation (30), and γ_n (dotted curve) calculated by equation (31) for each field line, which crosses the X axis at X . In the calculation of ω_{rn} and γ_n , we used $k_y = k_{ym} =$

L_p^{-1} . The growth rates γ and γ_n are not very different and decrease monotonically with $|X|$. At $X = -15 R_E$, $\gamma \sim \gamma_n$ becomes ~ 0.25 rad/s. Therefore the e-folding time of the ballooning modes becomes ~ 4 s. For the two component fluid case $\omega_{rn} \ll \gamma_n$ is satisfied and $2\pi\omega_{rn}^{-1} \sim 2330$ s at $X = -15 R_E$. We should note that the growth rate γ obtained analytically from equation (28) and shown in Figure 5 is almost equal to the exact growth rate γ_e calculated numerically by solving the eigenmode equation (7) (see Figure 6 of Miura *et al.* [1989]). More specifically, Figure 6 of Miura *et al.* [1989] gives $\gamma_e \sim 0.86 \gamma_{MHD}$ and therefore γ calculated analytically by equation (28) ($\gamma \sim 0.707 \gamma_{MHD}$) is a bit smaller ($0.86/0.707 = 1.22$ times smaller) than γ_e but is a very good approximation of γ_e .

[31] Figure 6 shows, as a function of X , ω_{ci} (dashed curve), ω_{bi} (dotted curve) for $\theta_{eq} = 30^\circ$, γ (solid curve), and γ_n (dot-dash curve), which is nearly equal to $|\omega_n| = (\omega_{rn}^2 + \gamma_n^2)^{1/2}$. The bounce frequency ω_{bi} is calculated for ions with the thermal velocity v_{ti} . Since the s dependence of $B(s)$ in equation (33) is not known, τ_{bi} given by equation (33) was calculated numerically by taking grid points on the field line from $s = 0$ to $s = s_m$. Although the $\omega_{bi} = 2\pi/\tau_{bi}$ curve shown in Figure 6 is not smooth, ω_{bi} is converging to the exact value, since an increase in the number of grid points along the field line gives a more accurate ω_{bi} . For practical comparison with other characteristic frequencies in Figure 6, the curve of ω_{bi} is smooth enough.

[32] This figure shows that although ω_{bi} decreases slightly with $|X|$ in $|X| < 17.5 R_E$, it increases with $|X|$ in $|X| > 17.5 R_E$. This is a completely opposite dependence on $|X|$ from that of the bounce frequency for the dipole field configuration [Hamlin *et al.*, 1961]. For the dipole field the bounce frequency decreases with an increase in $|X|$. This behavior of the bounce frequency as a function of $|X|$ for a highly stretched tail configuration can be explained physically as follows. For a highly stretched field line, the field intensity decreases along the field line with distance from the equator ($s = 0$) more rapidly than the gently curved dipole field line. This means that for a more highly stretched field line, the mirror point for a fixed energy particle with a fixed pitch angle at the equator becomes closer to the equator and the distance s_m becomes smaller. Therefore for a fixed

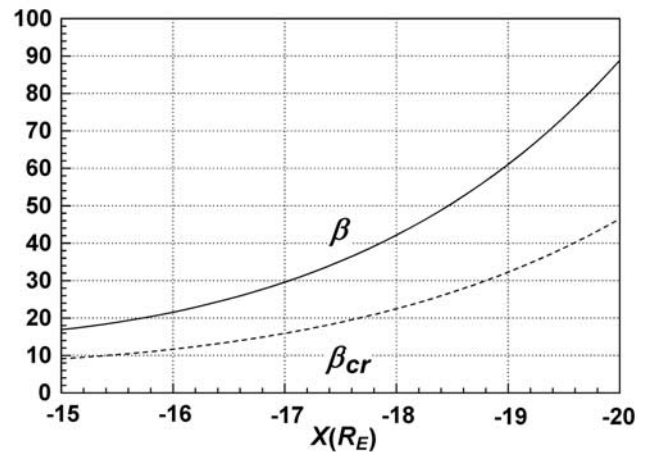


Figure 4. The plasma β calculated at the equator ($Z = 0$) and β_{cr} calculated by equation (29) as a function of X .

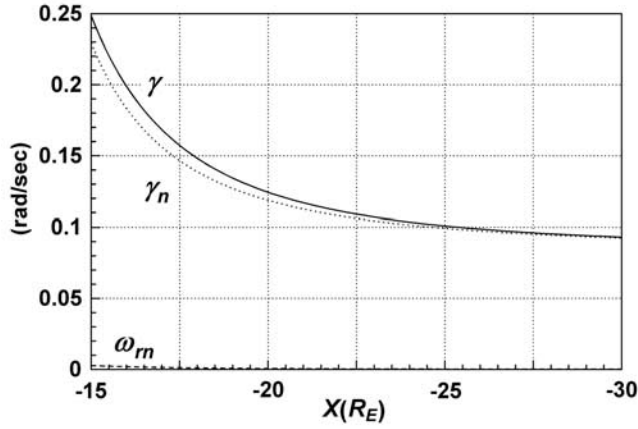


Figure 5. The γ (solid curve) calculated by equation (28), ω_{rm} (dashed curve) calculated by equation (30), and γ_n (dotted curve) calculated by equation (31) as a function of X for each field line, which crosses the X axis at X .

thermal ion velocity, the bounce time is expected to decrease with $|X|$, and hence ω_{bi} increases with $|X|$ for a highly stretched tail configuration. Hence ω_{bi} becomes larger than ω_{ci} at $|X| > 22 R_E$. The conservation of the ion's μ is expected to be valid when the particle bouncing motion is slower than the ion gyration motion, that is, when $\omega_{ci} > \omega_{bi}$. Therefore in $|X| > 22 R_E$, we expect that the ion motion becomes nonadiabatic and the ion's μ is not conserved. In $|X| > 23 R_E$, γ and γ_n become smaller than ω_{bi} . This means that in $|X| > 23 R_E$, the kinetic effects for ions with $\theta_{eq} = 30^\circ$ become important. At $|X| > 20.5 R_E$, γ and γ_n become larger than ω_{ci} . It is obvious that $\omega_{ci} > \gamma \sim |\omega_n| > \omega_{bi}$ is satisfied in $15 R_E < |X| < 20 R_E$. Therefore in $15 R_E < |X| < 20 R_E$, the bouncing effects by 30° pitch angle ions are negligible.

[33] Figure 7 is the same as Figure 6 except that $\theta_{eq} = 45^\circ$. Owing to the pitch angle increase, ω_{bi} is larger at all X than that shown in Figure 6 for $\theta_{eq} = 30^\circ$. This is because the mirror point is closer to the equator owing to the increase in θ_{eq} . Since we use the same number of grid points along the

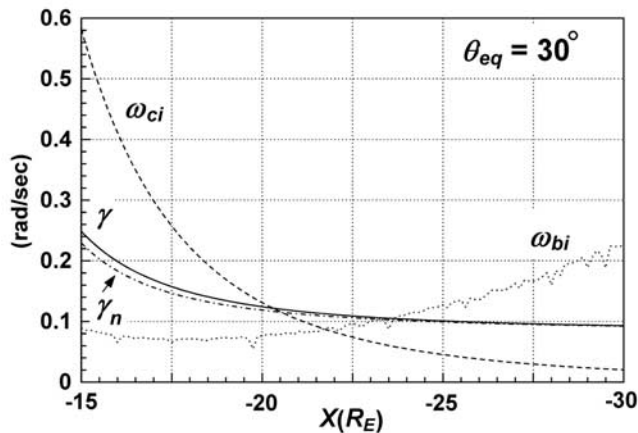


Figure 6. The ω_{ci} (dashed curve), ω_{bi} (dotted curve) for $\theta_{eq} = 30^\circ$, γ (solid curve), and γ_n (dot-dash curve), which is nearly equal to $|\omega_n| = (\omega_{rm}^2 + \gamma_n^2)^{1/2}$, as a function of X .

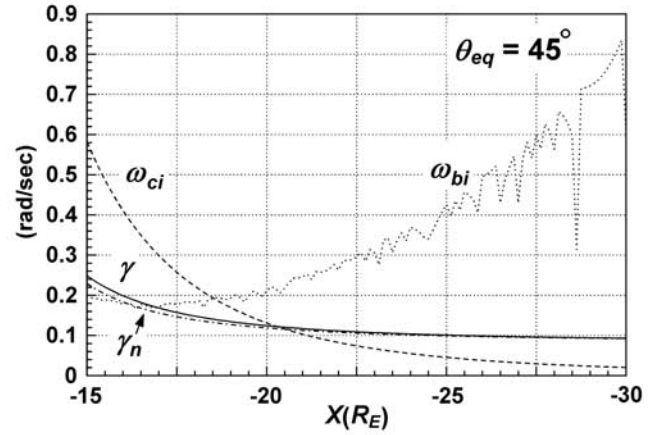


Figure 7. The same as Figure 6 except that $\theta_{eq} = 45^\circ$.

field line from the equator to the earthward boundary, the total number of grid points from $s = 0$ to $s = s_m$ decreases with a decrease in s_m . Therefore for a larger θ_{eq} , the substantial number of grid points for the calculation of ω_{bi} decreases and the convergence of ω_{bi} becomes worse. This is the reason why there is a large oscillation in ω_{bi} for $|X| > 20 R_E$ in comparison with Figure 6. In this case $\omega_{ci} > \gamma \sim \gamma_n \sim |\omega_n| > \omega_{bi}$ is satisfied at $15 R_E < |X| < 17 R_E$. Since ω_{bi} is larger than the previous case of $\theta_{eq} = 30^\circ$, the bouncing effects by these ions with $\theta_{eq} = 45^\circ$ become important in a wider region than the previous case of $\theta_{eq} = 30^\circ$. However, since γ and γ_n are still larger than ω_{bi} near $|X| \sim 15 R_E$, those bouncing influences by $\theta_{eq} = 45^\circ$ ions are negligible at $|X| \sim 15 R_E$. Also, the nonadiabatic effect due to $\omega_{bi} > \omega_{ci}$ becomes important in a wider region than the previous case.

[34] Figure 8 is the same as Figure 6 except that $\theta_{eq} = 60^\circ$. Owing to the pitch angle increase, ω_{bi} is larger at all X than that shown in Figure 7 for $\theta_{eq} = 45^\circ$. In this case $\gamma \sim \gamma_n \sim |\omega_n| > \omega_{bi}$ is not satisfied at all X . Therefore the bouncing effects by those ions with $\theta_{eq} = 60^\circ$ become important at all X . The nonadiabatic effect due to $\omega_{bi} > \omega_{ci}$ also becomes important in a wider region than the previous case of $\theta_{eq} = 45^\circ$ owing to the increase of ω_{bi} .

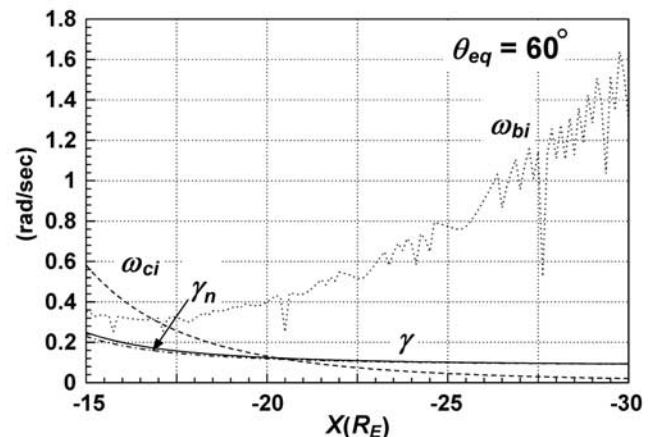


Figure 8. The same as Figure 6 except that $\theta_{eq} = 60^\circ$.

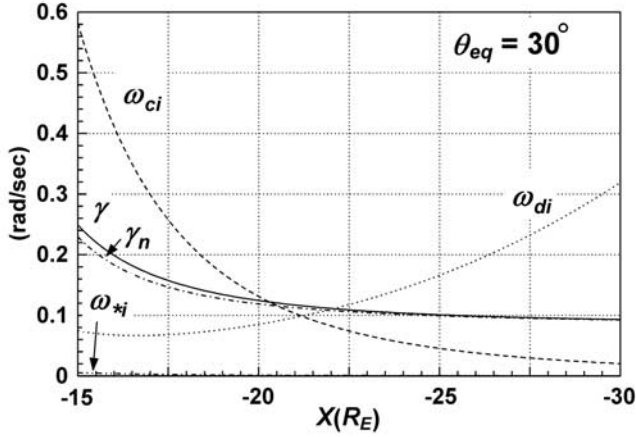


Figure 9. The ω_{ci} (dashed curve), ω_{di} (dotted curve) for $\theta_{eq} = 30^\circ$, ω_{*i} (double-dot dash curve), γ (solid curve), and γ_n (dot-dash curve) calculated at the equator as a function of X .

[35] Figure 9 shows, as a function of X , ω_{ci} (dashed curve), ω_{di} (dotted curve) for $\theta_{eq} = 30^\circ$, ω_{*i} (double-dot dash curve), γ (solid curve), and γ_n (dot-dash curve) calculated at the equator. Since ω_{di} is dominated by the curvature drift owing to the condition $R_c \ll R_b$, ω_{di} is almost determined by the curvature drift. Therefore ω_{di} increases with $|X|$ at $|X| > 17.5 R_E$ because of the decrease in R_c . In $|X| < 22 R_E$, $\gamma \sim \gamma_n \sim |\omega_n| > \omega_{di} > \omega_{*i}$ is satisfied. Therefore in $|X| < 22 R_E$, kinetic effects due to the ion magnetic drift can be neglected. The ion diamagnetic drift frequency $\omega_{*i} \sim 0.005$ is much smaller than ω_{di} in the present case. This is because ω_{*i} is proportional to L_p^{-1} .

[36] Figure 10 is the same as Figure 9, except that $\theta_{eq} = 45^\circ$. In this case ω_{di} is smaller than the previous case of $\theta_{eq} = 30^\circ$, since the curvature drift velocity becomes smaller in equation (35) than the previous case. Therefore in this case, the region where kinetic effects due to the ion magnetic drift can be neglected for the wave growth becomes wider than the previous case shown in Figure 9.

[37] Figure 11 is the same as Figure 9 except that $\theta_{eq} = 60^\circ$. In this case ω_{di} is smaller than the previous case of $\theta_{eq} =$

45° , since the curvature drift becomes smaller in equation (35) than the previous case.

7. Validity of the Fluid Description for the Ballooning Instability Onset

[38] When $|\omega|$ or $|\omega_n|$ of ballooning modes is smaller than the bounce frequency of particles, the particles bounce back and forth along the field line during the time period of $|\omega|^{-1}$. Therefore the use of a local electric field adopted in the fluid description is not valid, and we must use the bounce-averaged electric field, which largely differs from the local electric field. Figures 6–8 show that $\gamma \gg \omega_{bi}$ is valid in $|X| < 23 R_E$ for 30° pitch angle ions, $\gamma > \omega_{bi}$ in $|X| < 17 R_E$ for 45° pitch angle ions, but $\gamma < \omega_{bi}$ at all X for 60° pitch angle ions. Although 60° pitch angle ions divide the phase space volume in half, ω_{bi} depends sensitively on the pitch angle. Since the validity of the fluid description is determined by averaging over the particle distribution function, we calculate the average bounce frequency at $X = -15 R_E$, i.e., at the near-Earth tail.

[39] Since in the present calculation we calculate numerically the ion bounce frequency $\omega_{bi}(v_{ti}, \theta_{eq})$, we need to derive the average ion bounce frequency $\bar{\omega}_{bi}$ from numerically calculated $\omega_{bi}(v_{ti}, \theta_{eq})$. Since ω_{bi} is proportional to the ion velocity $v = |v|$, we obtain

$$\omega_{bi}(v, \theta_{eq}) = (v/v_{ti})\omega_{bi}(v_{ti}, \theta_{eq}). \quad (39)$$

Therefore by assuming an isotropic Maxwellian distribution the average ion bounce frequency $\bar{\omega}_{bi}$ averaged over the velocity distribution function becomes

$$\bar{\omega}_{bi} = \frac{1}{(\sqrt{\pi}v_{ti})^3} \int_0^\infty dv \int_0^{2\pi} d\varphi \int_0^\pi d\theta (v/v_{ti}) \cdot \exp(-v^2/v_{ti}^2) \omega_{bi}(v_{ti}, \theta) v^2 \sin\theta \quad (40)$$

where φ is the azimuthal angle in the velocity space and we dropped the subscript eq from θ_{eq} . After integration, equation (40) becomes simply

$$\bar{\omega}_{bi} = \frac{2}{\sqrt{\pi}} \int_0^{\pi/2} \omega_{bi}(v_{ti}, \theta) \sin\theta d\theta. \quad (41)$$

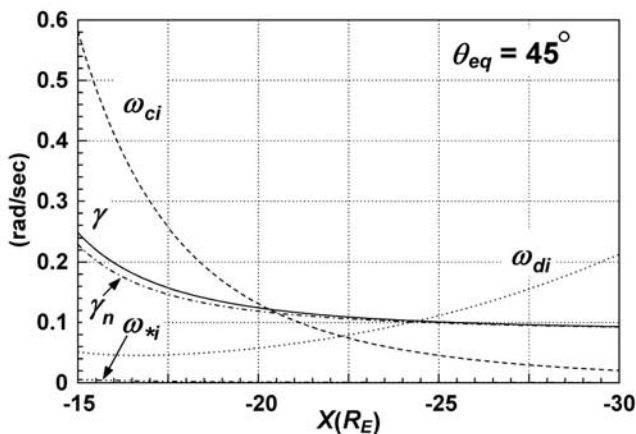


Figure 10. The same as Figure 9 except that $\theta_{eq} = 45^\circ$.

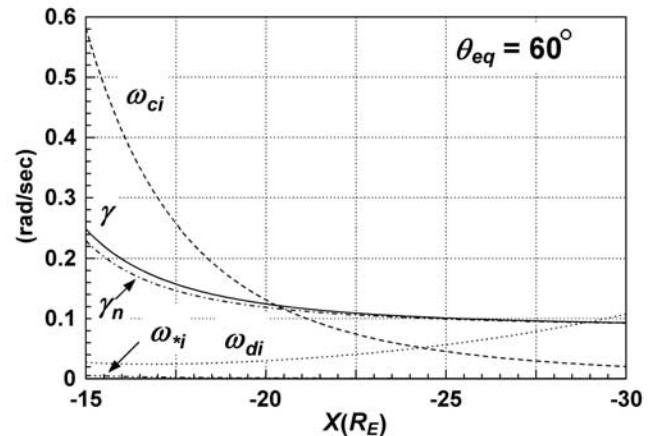


Figure 11. The same as Figure 9 except that $\theta_{eq} = 60^\circ$.

A finite difference approximation of equation (41) is

$$\bar{\omega}_{bi} = \frac{2}{\sqrt{\pi}} \sum_{j=1}^n \omega_{bi}(v_{ij}, \theta_j) \sin \theta_j \Delta\theta \quad (42)$$

where $\Delta\theta = \pi/(2n)$.

[40] We calculated $\omega_{bi}(v_{ij}, \theta_{eq})$ every 15 degrees by taking $n = 6$ and $\Delta\theta = \Delta\theta_{eq} = 15^\circ$ and obtained $\bar{\omega}_{bi} = 0.28$ rad/s by using equation (42). On the other hand, at $X = -15 R_E$ in Figure 5 the analytically obtained γ is ~ 0.25 rad/s. Since the exact growth rate γ_e obtained by the eigenmode analysis [Miura *et al.*, 1989] is 1.22 times larger than the analytically obtained γ , γ_e is ~ 0.305 rad/s. Therefore γ_e is larger than $\bar{\omega}_{bi}$ and the bouncing effects by these ions are neglected on average at $X = -15 R_E$. Although γ_e is not much larger than $\bar{\omega}_{bi}$ at $X = -15 R_E$, Figures 6–8 suggest that γ increases rapidly with decreasing $|X|$, whereas ω_{bi} stays nearly constant. Therefore the inequality $\gamma_e > \bar{\omega}_{bi}$ would be enhanced in $|X| < 15 R_E$.

[41] Kinetic influences by the magnetic drift can be neglected when

$$|\omega|/k_y \gg V_{di} > \langle v_{di} \rangle, \quad (43)$$

where $\langle v_{di} \rangle$ is the bounce average of the magnetic drift velocity, which is smaller than $v_{di} = V_{di}$ at the equator, since the curvature drift dominates in the magnetic drift and the curvature is maximal at the equator. The condition in equation (43) can be rewritten as $|\omega| \gg k_y V_{di} = \omega_{di}$ at the equator. When $|\gamma| \gg |\omega_r|$, this means that the Doppler shift due to the magnetic drift does not significantly affect the wave growth. When $|\gamma| \ll |\omega_r|$, this means that the wave phase velocity is much faster than the magnetic drift velocity and thus the drift resonance effect can be negligible. For all pitch angle ions shown in Figures 9–11, $\gamma > \omega_{di}$ is valid in $|X| < 24 R_E$. Therefore in this case there is no need to calculate the phase space average $\bar{\omega}_{di}$ and it is obvious that $\gamma_e > \gamma > \bar{\omega}_{di}$ at the near-Earth tail ($X = -15 R_E$). However, Figures 9–11 show that as in the case of bouncing effects by bouncing motion, the kinetic effects of the magnetic drift become more and more important as $|X|$ increases.

[42] Although ω_{*i} increases with a decrease in $|X|$ due to a decrease of L_p , ω_{*i} is much smaller than γ at all X and $|\omega| \gg \omega_{*i}$ is satisfied at all $|X|$ as long as $|X| > 15 R_E$. According to Büchner and Zelenyi [1989], the adiabatic assumption for ion motion is valid as long as $R_c > \rho_{Li}$. However, the specific detail of when μ conservation is violated at what R_c/ρ_{Li} depends on a tail model. We conjecture that when $\omega_{bi} > \omega_{ci}$, the ion motion becomes nonadiabatic because the formula of τ_{bi} calculated by equation (33) is based on conservation of μ . Figure 12 shows as a function of θ_{eq} the ratios of $\kappa^2 = R_c/\rho_{Li}$ and $\kappa^{*2} = \omega_{ci}/\omega_{bi}$ calculated at the equator at $X = -15 R_E$. Although they are different, they decrease with an increase in θ_{eq} . This suggests that like $\kappa^2 = R_c/\rho_{Li}$, $\kappa^{*2} = \omega_{ci}/\omega_{bi}$ is also a good measure of the validity of the ion adiabaticity in a tail model. The equivalence of the ion bounce/ion gyrofrequency ratio to the Larmor radius/field line curvature ratio as a condition for nonadiabatic ion motion has been noted by Büchner and Zelenyi [1989]. Equation (9) of Büchner and Zelenyi [1989] shows that the ratio of the

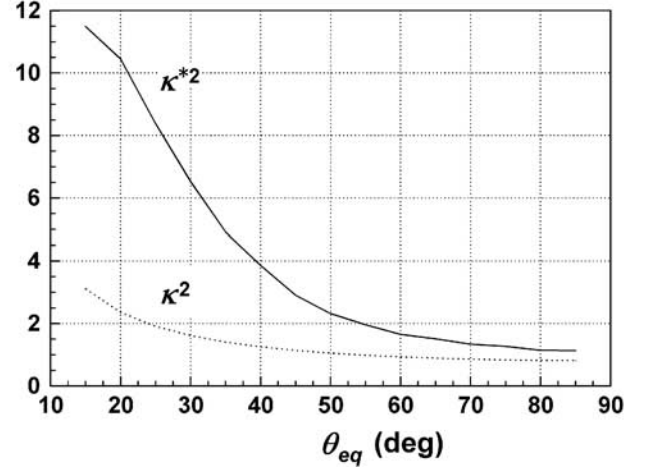


Figure 12. The ratios of $\kappa^2 = R_c/\rho_{Li}$ and $\kappa^{*2} = \omega_{ci}/\omega_{bi}$ calculated at the equator at $X = -15 R_E$ as a function of θ_{eq} .

gyrofrequency at the midplane to the largest possible bounce frequency of small amplitude linear guiding center oscillations around the equatorial plane, which is obtained by expanding the potential function in the Hamiltonian around the midplane, is equal to κ^2 . However, Figure 12 shows that the ratio of the gyrofrequency at the midplane to the numerically calculated exact ion bounce frequency (nonlinear oscillation frequency), which is defined as κ^{*2} , is larger than κ^2 for the present tail model. Since we consider that when $\omega_{bi} > \omega_{ci}$ the conservation of the ion's μ is violated, Figures 6–8 show that the adiabatic region in the near-Earth tail decreases with an increase in θ_{eq} . This is also reasonable because the ion Larmor radius increases with an increase in θ_{eq} . This nonadiabatic or stochastic effect for ion motion also becomes more and more important as $|X|$ increases. We find in Figure 7 that at $X = -15 R_E$ the adiabatic assumption for ion motion is valid for 45° pitch angle ions. The ion stochastic effect is to change the equation of state. Since it has been shown by Miura [2000] using a MHD-like formulation of Hurricane *et al.* [1995] that for stochastic plasmas the equation of state can be replaced by the incompressible equation for a ballooning mode strongly localized near the equator, this stochastic effect might not severely affect the fluid description like other kinetic effects seen above.

[43] Therefore as far as the present tail model is concerned, the fluid description is valid in the near-Earth tail at $X \sim -15 R_E$, since the condition $|\omega| > \bar{\omega}_{bi}$, $\bar{\omega}_{di}$, ω_{*i} is satisfied and the ion motion is adiabatic at $X \sim -15 R_E$.

8. Discussion

8.1. Comparison With Simulation Results

[44] Pritchett and Coroniti [1999] did a full particle 3-D simulation of the ballooning instability in the convectively driven near-Earth plasma sheet, in which the $|X|$ -variation is restricted to the range of ~ 6 – $11 R_E$. They observed an initiation of the ballooning instability in the middle of the X range when local plasma β exceeds ~ 16 . The β_{cr} calculated from $\beta_{cr} = L_p/R_c$ was ~ 9 . Therefore there is an important difference between β_{cr} and the observed critical β . Since their study is considered to be simulating

a development of the two component fluid ballooning instability or the drift ballooning instability, their simulation follows the development of a mode with $\omega = \omega_{rn} + i\gamma_n$. They found $\gamma_n \sim 0.06\omega_{ci}$ and $\omega_{rn} \sim 0.07\omega_{ci}$. The reason why they had such a large ω_{rn} is because they simulated a region much closer to the Earth than the present study, where the pressure gradient is larger. Figure 5 shows that in the present model $2\pi\omega_{rn}^{-1} \sim 2330$ s or $\omega_{rn} \sim 0.0047\omega_{ci}$ at $X = -15 R_E$. Since the real frequency ω_{rn} is proportional to ω_{*i} , it is proportional to $B_0^{-1}\nabla p_0$. Although B_0 increases with decreasing distance, ∇p_0 increases more rapidly than B_0 , and therefore we expect that ω_{rn} increases with decreasing distance from the Earth. Such a tendency can be seen in Figure 5, where ω_{rn} increases with decreasing distance. It is not certain whether such a large increase of ω_{rn} with decreasing $|X|$ could explain short period diamagnetic hydromagnetic oscillations with periods of ~ 45 – 65 s, which are observed during the most active phase of the substorm breakup within $10 R_E$ from the Earth [Holter *et al.*, 1995].

[45] For $R_c \ll R_b$, substitution of equation (27) into equation (31) and using equation (30) yield

$$\gamma_n^2 = \frac{V_A^2}{R_c^2} - \omega_{rn}^2. \quad (44)$$

Therefore we obtain from equations (32) and (44) that

$$\beta_{cm} = \beta_{cr} \frac{\gamma_n^2 + 2\omega_{rn}^2}{\gamma_n^2 + \omega_{rn}^2}. \quad (45)$$

For the fastest growing mode $k_{ym}L_p = 1$ is expected. Therefore when T_i and T_e are uniform, we obtain for the fastest growing mode

$$\omega_{*i} = \frac{k_y}{eB_0} \frac{kT_i}{L_p}. \quad (46)$$

Therefore equation (32) can also be written as

$$\beta_{cm} = \beta_{cr} \left[1 + \frac{R_c^2}{4V_A^2} \left(\frac{kT_i}{eB_0} \frac{1}{L_p} \right)^2 \right]. \quad (47)$$

If we use $\gamma_n/\omega_{rn} = 6/7$ and $\beta_{cr} = L_p/R_c \sim 9$ obtained by the simulation [Pritchett and Coroniti, 1999], we obtain $\beta_{cm} \sim 17$ from equation (45). This gives an excellent agreement with observed critical β of 16 in their simulation. Therefore their simulation results, showing a larger critical β than $\beta_{cr} = L_p/R_c$, can be explained by the development of a two component fluid ballooning mode, which has a critical β given by equation (32) larger than $\beta_{cr} = L_p/R_c$. From equation (44) and their observed γ_n and ω_{rn} we also obtain $\gamma_n = 0.862V_A/R_c$. Therefore in their simulation the ballooning mode is really growing with an Alfvén time scale $\tau_A \sim R_c/V_A$.

[46] In their simulation, a mode with $\lambda_y = 128 \Delta$, where Δ is the grid spacing, had the largest growth rate. When averaged over the growing time their simulation showed that at the location of the development of the ballooning mode, $\rho_{Li} \sim 16 \Delta$ and $L_p \sim 50 \Delta$. As has been described in

section 5 the fastest growing mode is expected to occur at $k_{ym}L_p \sim 1$. Therefore a ballooning mode having $\lambda_{ym} = 2\pi L_p \sim 314\Delta$ is expected to grow fastest. The observed λ_y in their simulation is less than half of λ_{ym} . This discrepancy may be due to the fact that $k_{ym}L_p \sim 1$ is a crude estimation or it may be due to the neglect of full FLR effects, which have not been incorporated in the present two component fluid description. It should be emphasized that in their simulation a mode with $\lambda_y = 128 \Delta = 8\rho_{Li} ((k_{\perp}\rho_{Li})^2 = 0.64 < 1)$ grew fastest. Therefore the initial mode destabilized by the ballooning instability has a wavelength much larger than the ion Larmor radius.

[47] Although the present two component fluid model does not calculate δp_e , Cheng and Lui [1998] calculated the perturbed electron distributions based on the electron gyrokinetic formulation because of $|\omega| < \omega_{be}$ and argue that the critical β increases drastically by the parallel electric field due to electron trapping effects. For ions they assume, without testing its validity, that $|\omega|/k_{\parallel} > v_{ti}$, which is equivalent to $|\omega| > \omega_{bi}$. Their calculated β_{crkin} (critical β of kinetic ballooning instability) is given by

$$\beta_{crkin} = S\beta_{cr} + \frac{\omega_{*pi}^2 R_c L_p}{4(1+b_i)V_A^2}, \quad (48)$$

where $b_i = (k_{\perp}\rho_{Li})^2/2$ and $\omega_{*pi} \sim \omega_{*i}$. Here, S appears owing to the electron trapping effect and depends on the mirror ratio between the ionosphere and the equator and also on the electron mass (compare equation (48) with equation (32)). According to their calculation S is in the order of $100 \sim 1000$. Since they assume $\beta_{cr} \sim 0.2$, β_{crkin} becomes $\sim O(10)$, which is comparable to observed β in the near-Earth plasma sheet. However, $\beta_{cr} \sim 0.2$ seems to be too small in the near-Earth high β plasma sheet prior to a substorm onset. Indeed, it is in the order of 10 in the present calculation and in the simulation of Pritchett and Coroniti [1999]. If we substitute $\beta_{cr} \sim 10$ into equation (48), β_{crkin} becomes $O(10^3)$. Such a large critical β due to the electron trapping effect has not been observed by the simulation of Pritchett and Coroniti [1999] including full electron kinetics. However, although a fairly large mirror ratio is chosen in the simulation of Pritchett and Coroniti [1999], they used a mass ratio $m_i/m_e = 16$. Since S depends on the electron mass, the simulation of Pritchett and Coroniti [1999] may not fully explore the parameter regime, where the electron trapping effect may become important.

8.2. Upper Critical β for the Validity of $\gamma < \omega_{ci}$

[48] The condition $\gamma > \omega_{ci}$ means a violation of the ion magnetic moment μ conservation by the wave motion and that both ion and electron behave quite differently in a magnetic field and that the quasi-neutrality adopted in the fluid model may not be a good approximation. If equation (27) is valid, $\gamma < \omega_{ci}$ can be written by using equations (8) and (28) as

$$\beta < 2L_p\omega_{pi}/c, \quad (49)$$

where c is the light speed, ω_{pi} is the ion plasma frequency, and c/ω_{pi} is the ion inertial length. Therefore the condition $\gamma < \omega_{ci}$ gives an upper critical β equal to $2L_p\omega_{pi}/c$. Since

Figure 6 shows that $\gamma < \omega_{ci}$ is well satisfied near $X \sim -15 R_E$, β is much smaller than $2L_p\omega_{pi}/c$ near $X \sim -15 R_E$.

8.3. Onset Time Scale

[49] Since the inverse of the ballooning growth rate gives an e-folding time of the Alfvén wave amplitude, this e-folding time or the Alfvén time scale $\tau_A \sim R_c/V_A$ should characterize the onset time scale of the sudden substorm onset, if the ballooning onset really corresponds to the substorm onset. Therefore the observed parameter, which is most relevant to the present theory and perhaps most important for clarifying the substorm onset mechanism, is the rising time scale of the sudden substorm onset (“onset time scale” or “onset time constant”). *Liou et al.* [1999] give observations of auroral luminosity changes at the substorm onset. According to their Figures 1 and 2, the integrated photon flux over an area of 10 magnetic latitudes in the premidnight local time has an e-folding rising time of several tens of seconds. When the photon flux is calculated from each onset arc intensification from their Plates 1 and 3, which is a more accurate onset time scale than that of the integrated flux, the e-folding time becomes shorter. Although this e-folding time of the auroral luminosity is not necessarily the e-folding time of the Alfvén wave amplitude associated with the instability, it should be a good measure of the e-folding growth time of the instability responsible for the substorm onset. Therefore we may reasonably consider that the substorm “onset time scale” is several tens of seconds. Figure 5 shows that at $X = -15 R_E$, $\gamma^{-1} \sim \gamma_n^{-1} \sim 4$ sec. Therefore this rapid growth time of the ballooning instability can account for the observed onset time scale. It is important to notice that the present unstable (drift) Alfvén mode accompanies the parallel electric field for particle acceleration owing to the ∇p_e term in the generalized Ohm’s law and nonzero $\mathbf{e} \cdot \nabla = ik_{\parallel}$ (see (17)).

8.4. Direct Measurement of the Field Line Curvature Radius R_c at the Equator for the Calculation of β_{crn}

[50] For the present theory a most critical parameter in determining the growth rate and the critical β is the field line curvature radius R_c at the equator. The curvature radius R_c is important because R_c is the e-folding length of the strongly localized Alfvén mode decaying from the equator [*Miura et al.*, 1989]. Although obtaining the field line curvature radius at $Z \neq 0$ is difficult, R_c can be calculated easily at the equator, if the field lines are symmetric with respect to the equatorial plane, by using the following formula

$$R_c^{-1} = |(\mathbf{e} \cdot \nabla)\mathbf{e}|_{Z=0} = \left| \frac{1}{B_{0z}} \frac{\partial B_{0x}}{\partial Z} \right|_{Z=0}, \quad (50)$$

where $B_{0z}(X, Z = 0)$ is the normal component of the magnetic field at the equator. Therefore by using $\Delta B_{0x} = B_{0x}(X, L_z) - B_{0x}(X, 0) = B_{0x}(X, L_z)$ for small L_z , equation (50) can be calculated from observations by

$$R_c^{-1} \sim \frac{1}{B_{0z}(X, 0)} \frac{\Delta B_{0x}}{L_z}. \quad (51)$$

Although *Korth et al.* [1991] and *Pu et al.* [1992] calculated L_p and R_c from observations, their calculation of R_c relies on some model calculation of the field inflation by a finite

pressure plasma. Therefore the above direct measurement of R_c will give a more accurate calculation of β_{cr} or β_{crn} .

8.5. Limitations of the Present Model

[51] The present calculation excludes the most likely onset region ($6 \sim 12 R_E$ from the Earth). This is due to our choice of the tail equilibrium without the dipole field. This is a severe limitation of the present model when applied to the substorm onset mechanism and the present model calculation cannot answer where in the near-Earth magnetosphere a ballooning mode might at first be destabilized.

[52] If the tail changes very slowly from the stable state to a more stressed state during the preonset phase (late growth phase), the tail becomes first marginally stable when β becomes equal to β_{cr} . Thus a highly stressed tail would never be realized. Therefore in the present model it is assumed that somehow the tail evolves rapidly from the initial stable state to a highly stressed state (passing through the marginal state), in which the ballooning growth rate is much larger than the marginal one, since the tail is driven or forced to become more tail-like. Under such a situation, a growth rate much larger than the marginal state is attained. Of course, the possibility that the tail is put into a highly stressed state by passing through the marginal state has not been established and there are different scenarios based on nonlinearity such as a detonation hypothesis [*Hurricane et al.*, 1999]. The merit of the detonation scenario is that the detonation only requires that the system is near marginal stability and the onset time scale is that of an explosive nonlinearity. However, there has been no demonstration that the nonlinear detonation of ballooning in the stressed magnetotail is consistent with substorms. In this regard it is still worth pursuing the possibility of the explanation of the onset by a simple linear ballooning growth rate with the Alfvén time scale ($\tau_A \sim R_c/V_A$). It should be pointed out that in a particle simulation of ballooning instability by *Pritchett and Coroniti* [1999], the convectively driven system passes through the marginal stability region quickly and is brought into a regime where a large growth rate as predicted by the present theory ($\gamma \sim V_A/R_c$) has been observed. However, *Pritchett and Coroniti* [1999] also point out that a subsequent benign behavior of the ballooning in the nonlinear phase cannot mimic the development of a substorm. Therefore a simple nonlinear saturation of spontaneous ballooning instability cannot explain the substorm phenomena after the onset. This may be due to the nature of the forcing or driving of the system during the late growth phase prior to a substorm onset, which possibly depends on the nature of the solar wind-magnetosphere interaction. *Pritchett and Coroniti* [1999] argue that the failure to observe the predicted detonation behavior of the ballooning instability in their simulation may be a consequence of the simulation system being driven too fast and the dimensions being too small.

9. Summary and Conclusion

[53] For a realistic 2-D tail configuration satisfying $R_c \ll R_b$, the growth rates and the real frequencies of MHD ballooning modes, ω_{bi} , ω_{di} , ω_{*i} , and ω_{ci} are calculated numerically at the equator as a function of X from the near-Earth tail ($X = -15 R_E$) to the mid tail ($X = -30 R_E$).

The growth rates increase monotonically with decreasing $|X|$, ω_{bi} increases with increasing $|X|$, and ω_{di} dominated by the curvature drift frequency also increases with increasing $|X|$, because R_c decreases with increasing $|X|$. The exact growth rates of ballooning modes $\gamma_e \sim \gamma_{ne} \sim 1.22V_A/R_c$ satisfy $\bar{\omega}_{bi}, \bar{\omega}_{di}, \omega_{*i} < \gamma_e < \omega_{ci}$ in the near-Earth tail at $X \sim -15 R_E$, where $\bar{\omega}_{bi}$ and $\bar{\omega}_{di}$ are ω_{bi} and ω_{di} averaged over the distribution function. This validity condition of MHD tends to be more enhanced with decreasing $|X|$ from $X \sim -15 R_E$. Also, the ion motion remains adiabatic and the magnetic moment μ is conserved in the near-Earth tail at $X \sim -15 R_E$.

[54] Therefore it is a posteriori verified that the fluid or MHD description of the linear stability of the ballooning instability is valid in the near-Earth tail as close as $15 R_E$ from the Earth and the critical β and the Alfvén time scale $\tau_A \sim R_c/V_A$ of the ballooning instability onset are validated. There is excellent agreement between the critical β and the Alfvén time scale obtained analytically for the drift ballooning mode and those obtained by a 3-D particle simulation. This agreement further supports the validity of the fluid description of the ballooning instability onset in the near-Earth tail. Despite the plasma being collisionless and high- β in the near-Earth tail, the subtle collisionless kinetic effects are not significant enough to invalidate the fluid description in the near-Earth tail at $X \sim -15 R_E$. The Alfvén time scale of an e-folding growth of the drift Alfvén wave trapped within a field line curvature radius R_c in the equatorial region is in the order of a few tens of seconds or less in the near-Earth tail and is faster than the bounce time of the bulk of ions and can explain the observed rapid time scale of a substorm onset. Therefore the local characteristics of the substorm onset in the near-Earth tail, such as the rapid onset time scale, can well be explained by the onset of the ballooning instability in the fluid or MHD regime including the ion diamagnetic drift effect (drift ballooning regime) in the near-Earth plasma sheet. Unless the ballooning instability in the near-Earth plasma sheet occurs in the fluid regime, the ballooning instability would not cause any macroscopic influence on the pressure balance nor cause a macroscopic “onset” which would disrupt the near-Earth pressure balance. Although a subsequent development after the onset is beyond the scope of the present linear analysis, the highly stretched field lines beyond the near-Earth plasma sheet may tend to collapse toward the near-Earth region, when the pressure balance in the near-Earth plasma sheet is suddenly disturbed by the onset of ballooning instability.

[55] Important simplifications and limitations of the present study are as follows:

[56] 1. The most likely onset region ($6-12 R_E$ from the Earth) of substorms is excluded from the present model, since the dipole field component in the near-Earth is not included in the present self-consistent 2-D field and plasma model.

[57] 2. Although the present two component fluid description takes into account the lowest order correction of FLR effects of ions as a FLR fluid term, i.e., the ion diamagnetic drift, full FLR effects are not taken into account. While the present calculation shows that the collisionless kinetic effects due to the field line curvature in high- β plasma become more and more important as $|X|$

increases, a kinetic description of plasmas, such as has been pursued in other studies, has not been investigated.

[58] 3. Although the present two component fluid analysis of ballooning instability allows the existence of a parallel electric field for auroral electron acceleration at the onset by the existence of ∇p_e in the generalized Ohm’s law, the parallel electric field is not evaluated, since δp_e has not been calculated. The electron trapping effect, which has been obtained by calculating δp_e using the electron gyro-kinetic equation, is not taken into account.

[59] Although the present calculation includes certain simplifications, it eliminates important restrictions of the fluid or MHD description of ballooning instability, which have long been obstacles in applying it to the near-Earth collisionless high- β plasma sheet.

[60] **Acknowledgments.** This work was supported by Grants-in-Aid for Scientific Research 14540414. The computation portion of this work was supported by Radio Atmospheric Science Center of Kyoto University and Japan Aerospace Exploration Agency as a joint research project. The computation for this work was performed at Information Technology Center, University of Tokyo.

[61] Lou-Chuang Lee thanks Omar A. Hurricane and two other reviewers for their assistance in evaluating this paper.

References

- Bernstein, I. B., E. A. Frieman, M. D. Kruskal, and R. M. Kulsrud (1958), An energy principle for hydromagnetic stability problems, *Proc. R. Soc. London*, *A277*, 17.
- Bhattacharjee, A., Z. W. Ma, and X. Wang (1998), Ballooning instability of a thin current sheet in the high-Lundquist-number magnetotail, *Geophys. Res. Lett.*, *25*, 861.
- Büchner, J., and L. M. Zelenyi (1989), Regular and chaotic charged particle motion in magnetotail-like field reversals: 1. Basic theory of trapped motion, *J. Geophys. Res.*, *94*, 11,821.
- Chen, J. (1992), Nonlinear dynamics of charged particles in the magnetotail, *J. Geophys. Res.*, *97*, 15,011.
- Chen, L., and A. Hasegawa (1991), Kinetic theory of geomagnetic pulsations: 1. Internal excitations by energetic particles, *J. Geophys. Res.*, *96*, 1503.
- Cheng, C. Z., and A. T. Y. Lui (1998), Kinetic ballooning instability for substorm onset and current disruption observed by AMPTE/CCE, *Geophys. Res. Lett.*, *25*, 4091.
- Coppi, B. (1977), Topology of ballooning modes, *Phys. Rev. Lett.*, *39*, 939.
- Dubyagin, S. V., V. A. Sergeev, C. W. Carlson, S. R. Marple, T. I. Pulkkinen, and A. G. Yahnin (2003), Evidence of near-Earth breakup location, *Geophys. Res. Lett.*, *30*(6), 1282, doi:10.1029/2002GL016569.
- Erickson, G. M., N. C. Maynard, W. J. Burke, G. R. Wilson, and M. A. Heinemann (2000), Electromagnetics of substorm onsets in the near-geosynchronous plasma sheet, *J. Geophys. Res.*, *105*, 25,265.
- Fairfield, D. H. (1987), Structure of the geomagnetic tail, in *Magnetotail Physics*, edited by A. T. Y. Lui, p. 23, Johns Hopkins University Press, Baltimore, Md.
- Frank, L. A., and J. B. Sigwarth (2000), Findings concerning the positions of substorm onsets with auroral images from the Polar spacecraft, *J. Geophys. Res.*, *105*, 12,747.
- Freidberg, J. P. (1987), *Ideal Magnetohydrodynamics*, Plenum, New York.
- Freidberg, J. P., and B. M. Marder (1973), Stability of two-dimensional magnetohydrodynamic equilibria, *Phys. Fluids*, *16*, 247.
- Gold, T. (1959), Motions in the magnetosphere of the Earth, *J. Geophys. Res.*, *64*, 1219.
- Hamlin, D. A., R. Karplus, R. C. Vik, and K. M. Watson (1961), Mirror and azimuthal drift frequencies for geomagnetically trapped particles, *J. Geophys. Res.*, *66*, 1.
- Hazeltine, R. D., and F. L. Waelbroeck (1998), *The Framework of Plasma Physics*, Perseus, Reading, Mass.
- Holter, Ø., C. Altman, A. Roux, S. Perraut, A. Pedersen, H. Pecseli, B. Lybekk, J. Trulsen, A. Korth, and G. Kremser (1995), Characterization of low frequency oscillations at substorm breakup, *J. Geophys. Res.*, *100*, 19,109.
- Horton, W., H. V. Wong, and J. W. Van Dam (1999), Substorm trigger conditions, *J. Geophys. Res.*, *104*, 22,745.
- Horton, W., H. V. Wong, J. W. Van Dam, and C. Crabtree (2001), Stability properties of high-pressure geotail flux tubes, *J. Geophys. Res.*, *106*, 18,803.

- Hurricane, O. A., R. Pellat, and F. V. Coroniti (1994), The kinetic response of a stochastic plasma to low frequency perturbations, *Geophys. Res. Lett.*, *21*, 253.
- Hurricane, O. A., R. Pellat, and F. V. Coroniti (1995), A new approach to low frequency "MHD-like" waves in magnetospheric plasmas, *J. Geophys. Res.*, *100*, 19,421.
- Hurricane, O. A., B. H. Fong, S. C. Cowley, F. V. Coroniti, C. F. Kennel, and R. Pellat (1999), Substorm detonation, *J. Geophys. Res.*, *104*, 10,221.
- Jacquay, C. J., A. Sauvaud, and J. Dandouras (1991), Location and propagation of the magnetotail current disruption during substorm expansion: Analysis and simulation of an ISEE multi-onset event, *Geophys. Res. Lett.*, *18*, 389.
- Kan, J. R. (1973), On the structure of the magnetotail current sheet, *J. Geophys. Res.*, *78*, 3773.
- Korth, A., Z. Y. Pu, G. Kremser, and A. Roux (1991), A statistical study of substorm onset conditions at geostationary orbit, in *Magnetospheric Substorms*, *Geophys. Monogr. Ser.*, vol. 64, p. 343, edited by T. A. Potemra et al., AGU, Washington D. C.
- Le Contel, O., S. Perraut, A. Roux, and R. Pellat (2001), Plasma transport during substorm growth phase and relation to breakup, *Space Sci. Rev.*, *95*, 415.
- Lee, D.-Y. (1998), Ballooning instability in the tail plasma sheet, *Geophys. Res. Lett.*, *25*, 4095.
- Liou, K., C.-I. Meng, A. T. Y. Lui, P. T. Newell, M. Brittnacher, G. Parks, G. D. Reeves, R. R. Anderson, and K. Yumoto (1999), On relative timing in substorm onset signatures, *J. Geophys. Res.*, *104*, 22,807.
- Liou, K., C.-I. Meng, A. T. Y. Lui, P. T. Newell, and S. Wing (2002), Magnetic dipolarization with substorm expansion onset, *J. Geophys. Res.*, *107*(A7), 1131, doi:10.1029/2001JA000179.
- Lopez, R. E., D. G. Sibeck, R. W. McEntire, and S. M. Krimigis (1990), The energetic ion substorm injection boundary, *J. Geophys. Res.*, *95*, 109.
- Lui, A. T. Y., R. E. Lopez, B. J. Anderson, K. Takahashi, L. J. Zanetti, R. W. McEntire, T. A. Potemra, D. M. Klumpar, E. M. Greene, and R. Strangeway (1992), Current disruptions in the near-Earth neutral sheet region, *J. Geophys. Res.*, *97*, 1461.
- McNutt, R. L., Jr., P. S. Coppi, R. S. Selesnick, and B. Coppi (1987), Plasma depletion in the Jovian magnetosphere: Evidence of transport and solar wind interaction, *J. Geophys. Res.*, *92*, 4377.
- Miura, A. (2000), Conditions for the validity of the incompressible assumption for the ballooning instability in the long-thin magnetospheric equilibrium, *J. Geophys. Res.*, *105*, 18,793.
- Miura, A. (2001), Ballooning instability as a mechanism of the near-Earth onset of substorms, *Space Sci. Rev.*, *195*, 387.
- Miura, A., S. Ohtani, and T. Tamao (1989), Ballooning instability and structure of diamagnetic hydromagnetic waves in a model magnetosphere, *J. Geophys. Res.*, *94*, 15,231.
- Ohtani, S., A. Miura, and T. Tamao (1989), Coupling between the Alfvén and slow magnetosonic modes in an inhomogeneous finite- β plasma, II, Eigenmode analysis of localized ballooning interchange instability, *Planet. Space Sci.*, *37*, 579.
- Pritchett, P. L., and F. V. Coroniti (1999), Drift ballooning mode in a kinetic model of the near-Earth plasma sheet, *J. Geophys. Res.*, *104*, 12,289.
- Pu, Z. Y., A. Korth, and G. Kremser (1992), Plasma and magnetic field parameters at substorm onsets derived from GEOS 2 observations, *J. Geophys. Res.*, *97*, 19,341.
- Roux, A., S. Perraut, P. Robert, A. Morane, A. Pedersen, A. Korth, G. Kremser, B. Aparicio, D. Rodgers, and P. Pellinen (1991), Plasma sheet instability related to the westward traveling surge, *J. Geophys. Res.*, *96*, 17,697.
- Samson, J. C., L. R. Lyons, P. T. Newell, F. Creutzberg, and B. Xu (1992), Proton aurora and substorm intensifications, *Geophys. Res. Lett.*, *19*, 2167.
- Tang, W. M., and P. J. Catto (1981), Kinetic effects on ballooning modes in mirror machines, *Phys. Fluids*, *24*, 1314.
- Wu, C.-C., P. L. Pritchett, and F. V. Coroniti (1998), Hydromagnetic equilibrium and instabilities in the convectively driven near-Earth plasma sheet, *J. Geophys. Res.*, *103*, 11,797.

A. Miura, Department of Earth and Planetary Science, University of Tokyo, Hongo, 7-3-1, Bunkyo-ku, Tokyo 113-0033, Japan. (miura@eps.s.u-tokyo.ac.jp)